


A thin-shell shape adaptable composite metamaterial

Journal Article**Author(s):**

Sakovsky, Maria; Ermanni, Paolo 

Publication date:

2020-08-15

Permanent link:

<https://doi.org/10.3929/ethz-b-000438102>

Rights / license:

[Creative Commons Attribution 4.0 International](#)

Originally published in:

Composite Structures 246, <https://doi.org/10.1016/j.compstruct.2020.112390>

Funding acknowledgement:

608881 - ETH Zurich Postdoctoral Fellowship Program II (EC)

150729 - Optical measurement of three-dimensional surface displacement fields of morphing structures (SNF)



A thin-shell shape adaptable composite metamaterial

Maria Sakovsky^{a,*}, Paolo Ermanni^a

^a *Laboratory of Composite Materials and Adaptive Structures, ETH Zürich, Leonhardstrasse 21, 8092 Zürich, Switzerland*



ARTICLE INFO

Keywords:

Mechanical metamaterials
Shape adaptation
Thin-ply composites

ABSTRACT

Mechanical metamaterials undergoing extreme deformations span an ever-increasing design space of mechanical performance. However, achieving selective deformability in load-carrying metamaterials remains unexplored. Anisotropic thin fiber-reinforced composite shells, which are soft in bending and stiff axially, present an attractive option for addressing this challenge but are difficult to realize in practice due to fabrication complexity. In this work, an integrated fabrication technique enabling single-step curing of complex composite mechanical metamaterials is proposed. By using 3D-printed tooling and silicone spacers, composite assemblies can be cured in an autoclave without the need for post-cure bonding of individual shells. The technique reduces manufacturing times and eliminates adhesive bonds, which add mass to the structure and can be points of failure. The proposed technique is demonstrated on a modified rotating square auxetic metamaterial geometry, with fabricated prototypes withstanding up to 60% global tensile strains elastically. The composite anisotropy is, moreover, used to control the deformation mechanism in the metamaterial, thereby delaying failure of the structure and allowing tunability of elastic properties. This work sets the stage for the use of composites as a means of expanding the design space achieved by mechanical metamaterials for shape adaptation in lightweight, load-carrying applications.

1. Selective deformability in load-carrying lightweight structures

Mechanical metamaterials rely on the unique combination of their material and geometry to achieve mechanical properties not commonly found in nature, including negative engineering constants, improved impact resistance, and energy dissipation. Among these metamaterials are cellular structures composed of unit cells capable of large geometrical changes, often enabled through hinge/crease mechanisms or elastic instabilities in slender elements [1]. Owing to their large deformation capabilities, such metamaterials can undergo extreme dimensional changes entirely elastically [1–5]. Moreover, scaling laws developed for various stretching and bending-dominated mechanical metamaterials indicate that for a given stiffness, these architected solutions offer lighter designs than a continuous material [6]. Given the versatility of the design freedom offered by the combination of unit cell geometry and constituent material properties, the application of this approach to lightweight, shape adaptable structures is exceedingly promising.

Recent advances in additive manufacturing have made polymers an ideal choice for mechanical metamaterials by allowing for use of softer polymers in highly strained locations (i.e. hinges) and easily accommodating complex geometries [7,1]. Hence, polymer metamaterials

have found applications in soft robotics [8,9] and medical stents [10–12], where load bearing capability is not necessarily a driving requirement. However, their application in the aerospace field, such as for morphing wings [13–15] and large reconfigurable space structures [16–18], requires selective deformability in lightweight, load-carrying structures. Successful implementation of this demands significant augmentation of the design spaces offered by existing mechanical metamaterials.

Lightweight, thin fiber-reinforced polymer (FRP) composite shells present an attractive material choice for realizing the required hinges and slender elements for deformation, while simultaneously expanding the achievable design space through anisotropy of the material. By selecting metamaterial geometries in which the deformation mode is bending dominated, one can exploit the low achievable bending radii of ultra-thin FRP laminates [19] to yield high strength metamaterials without sacrificing deformability. In fact, several aspects of FRP mechanics demonstrate their potential for extreme mechanical properties. The anisotropy offered through layup design allows for precise control of the shell mechanical response including behavior not achievable in isotropic materials, such as bend-twist coupling [20,21]. Furthermore, the layup can be designed to exhibit variable stiffness behavior by programming multiple stable shapes into the shell each with different

* Corresponding author.

E-mail address: msakovsky@ethz.ch (M. Sakovsky).

stiffness responses [22,23]. Finally, thin shells allow for elastic buckling, also resulting in variable stiffness [24].

A significant challenge preventing the exploration of this design space is a practical one – the fabrication of complex FRP shell assemblies is costly and time-consuming. The state-of-the-art in fabricating such structures is a two-step process – manufacturing of individual shell elements in an autoclave cure and assembly using adhesives in a follow-on cure [13,14]. Airolidi et al., for example, have used such a process to prototype chiral FRP metamaterials for morphing wings [13]. While the process allows for precise assemblies, design space exploration and rapid design iteration is not feasible due to the large number of costly molds required. Furthermore, the adhesive can significantly increase the mass of the resulting metamaterial due to the large number of joints [25] and the bond lines are an inherently weak part of the structure where failure is likely to occur at relatively low global strains (i.e. dimensional changes of the material). Lastly, existing literature has yet to leverage ultra-thin composites, with ply-thicknesses below $\sim 70 \mu\text{m}$, in order to achieve large deformations through bending-dominated architectures.

This work addresses two research gaps associated with composite metamaterials through an initial feasibility study: fabrication of complex FRP assemblies allowing rapid design iteration and exploration of anisotropy use in metamaterials. A novel integral fabrication process for FRP metamaterials is proposed here to utilize the full shape-adaptivity potential of these geometries while exploiting the high strength of FRP shells. The process employs rapid prototyping techniques by using additively manufactured autoclave tooling and silicone spacers to cure the entire metamaterial assembly in a single autoclave process. The technique is demonstrated on a modified rotating square mechanism but can be easily extended to arbitrary geometries. Prototypes containing a periodic arrangement of these unit cells are fabricated from ultra-thin carbon fiber prepregs and experimentally tested to failure to demonstrate their high strain capabilities. Furthermore, the anisotropy at the material level (i.e. the fiber distribution) is used to achieve tailoring of the macro-scale metamaterial response. Through development of finite element models, it is shown that the response of the structures under study is predictable, despite the complex geometry and fabrication. The study presented here, demonstrates the fabrication of complex FRP mechanical metamaterials of high-quality with an unprecedented combination of mechanical properties.

2. Concept for high strain composite metamaterials

The geometry used for exploring the potential of composite metamaterials is based on the ubiquitous rotating square auxetic mechanism (Fig. 1(a)) [26]. The unit cell for the geometry is composed of four squares, connected to each neighbor via a single corner. In an idealized structure, these connections are infinitely small and form a hinge with a zero energy revolute mechanism in response to an applied tensile load. The structure can undergo deformations up to a 41.4% maximum global strain through the simultaneous rigid body rotation of the squares, resulting in a Poisson's ratio of $\nu = -1$ [26].

Here, the mechanism is adapted by replacing the idealized point hinges with thin FRP ligaments that connect square FRP hubs. The FRP structure is cured on polymer cores which dictate the hub shape. The cores are used as autoclave tooling for the laminates and can be optionally a part of the final structure (Fig. 1(b)). For example, they can provide surfaces for conductive or optical coatings for reconfigurable antennas and telescopes. Alternatively, the cores can be removed after cure to leave an FRP shell structure. As uniaxial tension is applied to the structure, the rotation of the hubs is enabled by bending of the ligaments. By designing the deformation mode in this composite metamaterial to be bending-dominated, high strain behavior is enabled by leveraging the small shell thickness of the composite material (on the order of 100–200 μm).

The geometry is parametrized by the edge length of the hubs, d ,

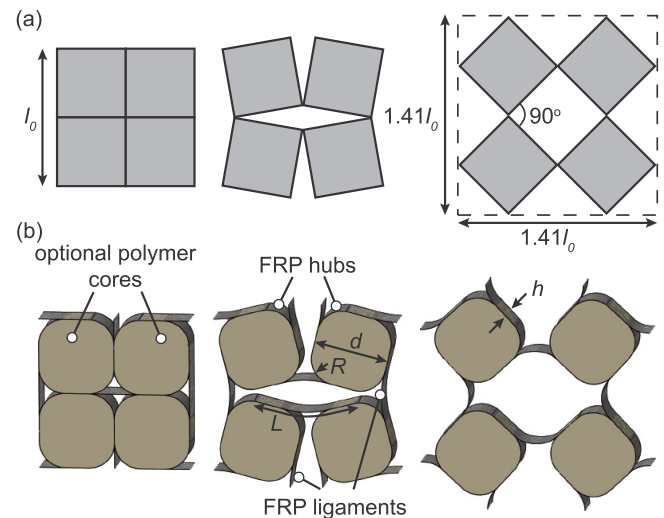


Fig. 1. Unit cell of the mechanical metamaterial geometry under study. (a) Original rotating square auxetic geometry. (b) Adapted FRP rotating square geometry in this study.

their corner radius, R , the length of the FRP ligaments, L , and the height of the metamaterial, h . By increasing the corner radius, the length of the ligament which is free to bend is increased, while by elongating the ligaments, the overlap with the FRP hubs is increased. As the metamaterial is an assembly of shells, the height can be a large fraction of the unit cell width, giving the metamaterial exceptional out-of-plane stiffness compared to existing polymer designs [1]. This study focuses on the effects of the composite material on metamaterial behavior and hence most geometric parameters are kept constant.

The geometry under study is representative not only of mechanisms based on rotating polygons, but also of other arrangements of hubs connected by ligaments, such as chiral geometries. In designs in literature, the hubs are assumed to be effectively rigid and the deformation is localized to the ligaments or hinges. It is shown that by using thin FRP shells, the design space can be extended by allowing both hub and ligament deformation and thereby achieving entirely novel mechanical behavior without modification of the geometry.

3. Integral fabrication of composite metamaterials

3.1. Process description

This work proposes a novel fabrication process that uses a single autoclave cycle to manufacture FRP mechanical metamaterials consisting of complex shell assemblies such as the one presented in Section 2. A schematic of the process is illustrated in Fig. 2(a). First, the cores, which shape the FRP hubs, are 3D-printed from a high temperature polymer capable of withstanding autoclave temperatures and pressures. If the cores are to be removed after cure, non-stick heat shrink (FEP heat shrink tubing with a wall thickness of 0.5 mm [27]) is applied to surround the cores and facilitate tooling removal. No additional release agent is required to remove the tooling.

The layup procedure begins by wrapping the prepreg layup of the FRP hubs around each core. The assembly starts at one corner of the structure by joining hubs with FRP ligaments according to the pattern in Fig. 2(a). Teflon film (Airtech Release Ease 234 TFNP PTFE coated fiberglass fabric) is used to allow separation of neighboring ligaments after cure and silicone spacers (Smooth-On Mold Max XLS II), molded to the shape of the gaps between hubs, are used to apply pressure during the autoclave cure [28]. Once the assembly is completed, it is wrapped in release film. Aluminum plates are placed around the perimeter of the structure to prevent the outer silicone spacers from buckling during

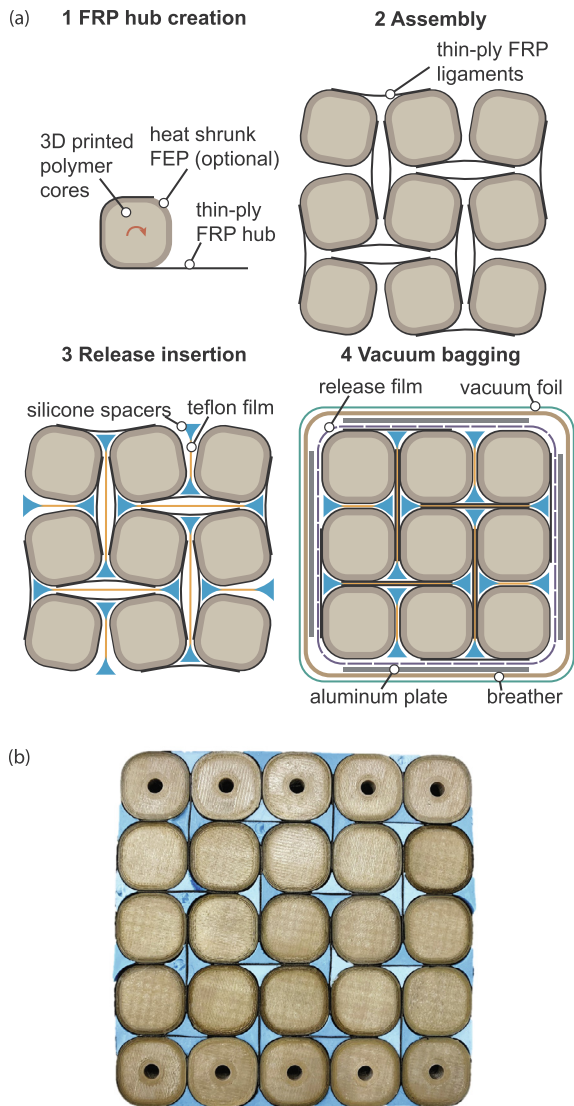


Fig. 2. Single cure fabrication procedure of FRP mechanical metamaterials. (a) Assembly procedure. (b) Assembled 5×5 rotating square metamaterial before cure.

cure and creating wrinkles on the outer ligaments. The whole assembly is then vacuum-bagged and cured in an autoclave. A photograph of a 5×5 assembly of hubs before cure, fabricated in this manner, is shown in Fig. 2(b).

The proposed fabrication procedure is extremely versatile. It is ideally suited for mechanical metamaterials composed of hub regions connected by ligaments, such as chiral geometries. However, this distinction between hubs and ligaments is not required and the procedure can be applied to any geometry that consists of an assembly of shells. Key to the methodology is a combination of 3D printed hubs and casted silicone spacers used for applying pressure to the prepreg to ensure consolidation of the material. Both of these components are compatible with a rapid prototyping approach, allowing many cost-efficient design iterations. The 3D-printed polymeric hubs also allow for the integration

of multi-functionality into the metamaterial. In the simplest case, their top and bottom surfaces can be used for functional coatings. Moreover, the 3D-printing process allows for the additional complexity to integrate mounts for sensors and to create mass optimized designs.

3.2. Materials

To demonstrate the fabrication technique, the tooling was 3D-printed from polyether ether ketone (PEEK) using the HPP 155 printer from Apium [29]. PEEK is a high performance polymer with a modulus of 4.0 GPa and a high glass transition temperature of 143 °C [30], making it ideally suited to handle autoclave temperatures and pressures.

The prototypes were manufactured using an ultra-thin 40 g/m² prepreg with M40J carbon fibers and 513 epoxy resin from North Thin-Ply Technologies [31]. The key material properties of the prepreg as well as its cure cycle are summarized in Table 1. The ultra-thin laminates are critical to the concept proposed here, as they allow for high curvatures of the ligaments before failure, thereby enabling extreme deformations of the stiff structure.

3.3. Prototypes

Metamaterial prototypes containing a 5×5 arrangement of hubs were fabricated to illustrate the feasibility of the proposed manufacturing technique. Various FRP layups and geometries were tested to investigate the tunability of the metamaterial structures (Table 2). Throughout the remainder of the paper, the samples are designated by their names in the first column of Table 2. This study focuses on the effects of the composite material rather than the geometry, since many studies in literature focus on metamaterial geometries [1]. Hence, all prototypes share the following geometry: $d = 22$ mm, $R = 7.5$ mm, and $h = 11$ mm. Only the effects of increasing the ligament length, L , are explored.

The ‘reference’ design has a uniform layup across the entire metamaterial and serves as a point of comparison for other designs. The FRP material opens the freedom for modification of the ligament and hub stiffness independently for control of the mechanics. This is illustrated by the ‘rigid hubs’ and ‘stiff hubs’ designs, which use polymer cores and a stiffer hub layup, respectively, to increase the hub stiffness relative to that of the ligaments (Table 2). Furthermore, the laminated material allows for an infinite combination of fiber angles to leverage the anisotropy for controlled deformation. Here, two anti-symmetric angle-ply layups are selected for the ligaments to demonstrate the use of the material to delay failure. Anti-symmetric layups are used to avoid bend-twist coupling, which would have a significant effect due to the bending-dominated architecture. The remaining coupling coefficients are negligible to the deformation as verified by finite element simulations (Section 4.2). The 45° angle-ply laminate has comparable bending stiffness to the cross-ply laminate used in the other samples, facilitating easy comparison between laminates. The 30° angle-ply laminate provides a sample where the bending stiffness of the ligaments is much higher than that of the hubs. Finally, the ‘long ligaments’ design increases the overlap between the ligaments and hubs, to gauge the effects of fabrication on failure of the metamaterial.

Fig. 3 shows a sample fabricated with the properties of the ‘reference’ design in Table 2. It can be seen that the polymer cores have been removed from the structure with the exception of the top and bottom rows where they enable interfacing with the testing apparatus

Table 1
Summary of key M40J/513 epoxy material properties [31,32].

Fiber modulus	Fiber strength	Resin modulus	Fiber volume fraction	Cure cycle
377 GPa	4.4 GPa	3.1 GPa	0.57	2 h. at 120 °C, 6 bar

Table 2
Summary of the geometry and layup of fabricated metamaterial prototypes investigated in present study.

Sample Name	Cores	Layup		L (mm)	Bending Stiffness (N·mm)	
		Ligaments	Hubs		Ligaments	Hubs
Reference	No	[0/90/0]	[0/90/0]	30	30.1	30.1
Long Ligaments	No	[0/90/0]	[0/90/0]	45	30.1	30.1
Rigid Hubs	Yes	[0/90/0]	[0/90/0]	30	30.1	~rigid
Stiff Hubs	No	[0/90/0]	[0/90 ₂ /0]	30	30.1	65.1
45° Angle-ply	No	[45/0 ₂ /-45]	[0/90/0]	30	27.4	30.1
30° Angle-ply	No	[30/0 ₂ /-30]	[0/90/0]	30	46.8	30.1

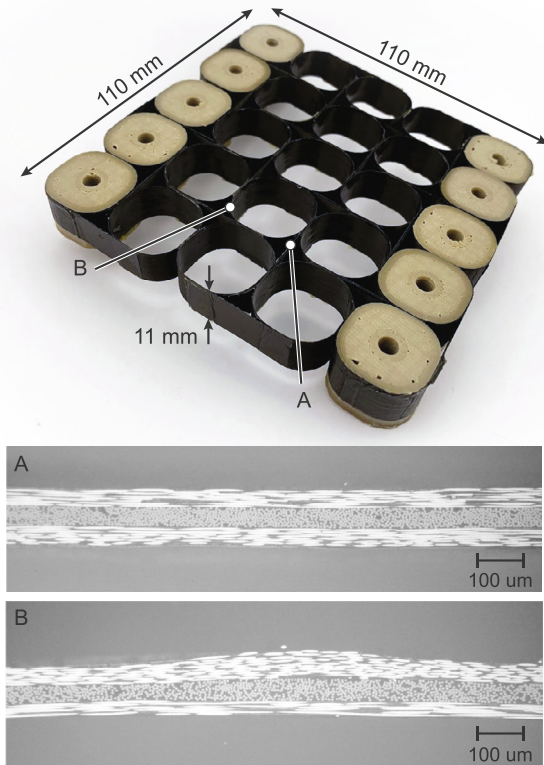


Fig. 3. 'Reference' prototype and micrographs of the FRP ligaments (A) and hubs (B).

(Section 4.1). This sample weighs only 6.2 g, excluding the PEEK interface for testing, illustrating the ultra-lightweight nature of the cellular material.

Micrographs of the fabricated samples (obtained with a Keyence VHX 6000 microscope) revealed that the average ligament ply thickness is 40 μm (2 μm standard deviation) (Fig. 3, panel A), while the average hub ply thickness is 39 μm (4 μm standard deviation) (Fig. 3, panel B). This is in good agreement with the expected ply thickness of 40 μm for the 40 g/m² prepreg. However, the average ply thickness of the outermost ligaments in the prototypes is 45 μm (2 μm standard deviation), 12% higher than for the other ligaments.

A uniform thickness is desired for the composite as thicker areas will result in higher strains and premature failure of the metamaterial. This is successfully achieved in the inner ligaments where the silicone spacers provide a uniform pressure, while the outermost ligaments see only the pressure of the vacuum bagging and not the neighboring hubs. This can be addressed by placing the assembly in a closed metal cage to apply a more uniform pressure throughout [28]. However, as will be demonstrated in Section 5.3, the outer ligaments are parallel to the applied load and therefore see lower bending radii compared to the inner ligaments. Hence, improving their thickness is not critical to the metamaterial performance in this case.

Finally, it should be noted that while a detailed study of the dimensional accuracy of the process was not conducted within the scope of this research, the outer dimensions of the prototypes were within 2% of the designed values. This error is a result of the difference in thermal expansion of the polymer cores and FRP material during the curing process. For high precision applications, the shape accuracy of the individual shells should be investigated in a follow-on study.

4. Methods

4.1. Tensile Testing of Metamaterials

The fabricated prototypes were subjected to a uniaxial tensile displacement until failure to examine the soft morphing mode of the structure. Thereby, the influence of geometry, material parameters, and fabrication on the elastic behavior and failure could be evaluated. The tests were conducted with a Zwick Roell Z005 material testing system using the custom-built tensile fixture shown in Fig. 4. Shafts with a 4 mm diameter were inserted through holes in the polymer cores left in the top and bottom rows of the prototypes (shown in Fig. 3). A ball bearing was mounted at each end of the shaft. The bearings could freely roll on rails in the top and bottom grips to allow transverse expansion of the metamaterial while permitting free rotation of the hubs. Lubricant was used to reduce the friction between the rails and bearings. All bearings at one end of the fixture were pinned by 3D-printed interfaces to remove rigid body motion.

The samples were loaded at 10 mm/min, to approximate static loading, with three loading cycles applied to each sample, first to a 10 mm extension, then to 20 mm and finally to ultimate failure. The reaction force was measured using a 5 kN load cell while the hub

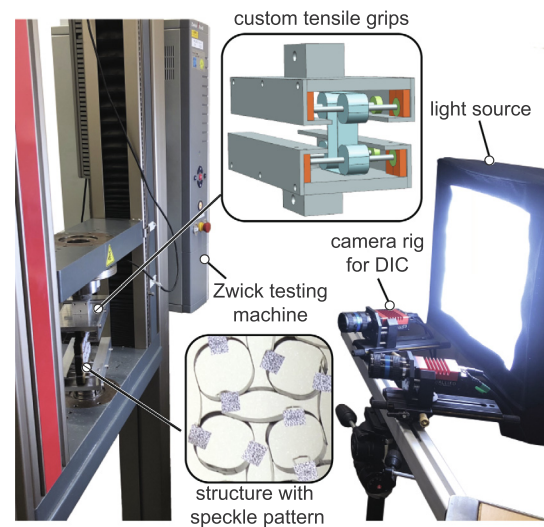


Fig. 4. Experimental setup for tensile testing of metamaterials. The insets show a close-up of custom built tensile grips and the distribution of DIC speckle targets in samples with cores removed.

deformation was captured using a 3D digital image correlation (DIC) system. Two AVT Prosilica GT3400 cameras, with LINOS MeVis-C 35 mm lenses, and a stereo angle of 22° were used to record images of the deformation and the VIC 3D 8 software was used for analysis. For the ‘rigid hubs’ samples, printed speckle patterns were glued directly to the polymer cores. This could not be done for the remaining samples to due the small thickness of the composite shells. Instead, random speckle patterns were printed and cut into $5 \times 5 \text{ mm}^2$ squares. These were glued to the tip of paper clips which were fixed to the flat portions of the hubs (Fig. 4 inset). This enabled measurement of the dimensional changes of the square hubs during metamaterial deformation without affecting the deformation or failure. Although simplistic, these markers were capable of tracking the movement of the hub edges and did not slip relative to the composite. Furthermore, the markers were placed on the straight sections of the FRP hubs, which do not deform significantly, thereby minimizing their effect on the deformation.

4.2. Finite element model

The elastic behavior of the composite structures was simulated using the commercial finite element software package ABAQUS 6.14 Standard (Fig. 5). The composite material was discretized using fully-integrated shell elements (S4) with the composite plies modeled as transversely isotropic with lamina properties derived from manufacturer data in Table 1 [31], while the overall shell behavior was computed from classical lamination theory using the built-in composite layup tool in ABAQUS. Three section points were used through-thickness to model the shells. The PEEK hubs were modeled as linearly elastic and isotropic using reduced integration 3D linear 8-node brick elements (C3D8R). A mesh size of 0.5 mm for the FRP and 1.0 mm for the polymer hubs was selected using a convergence study.

The interface between the FRP ligaments and hubs, as well as between the polymer hubs and FRP hubs, was approximated using tie constraints with all translational and rotational degrees of freedom constrained. This assumed that there was no delamination between these components during the elastic portion of the structure’s response. As will be shown in Section 5.2, this is sufficient to approximate the

elastic behavior but is not valid to predict failure, which the model did not attempt to do.

Boundary conditions were set to match experiments, with free rotation of all hubs as well as sliding in the direction transverse to loading allowed. The outermost hubs on one side of the metamaterials were pinned to remove rigid body motion. Lastly, to capture the effects of the large deformation, the non-linear geometry option was enabled in the solver, for accurate computation of the strains using the updated element area at each simulation increment [33].

Here, the applied strain was defined using a homogenized measure as,

$$\varepsilon_a = \frac{d_a}{4d} \quad (1)$$

and the transverse strain was defined as,

$$\varepsilon_t = \frac{d_t}{5d} \quad (2)$$

where d is the initial hub edge length, and d_a and d_t are the applied and transverse displacements as illustrated in Fig. 5. Note that the transverse displacement in Fig. 5 was defined to match the location of the DIC markers in the experiments. Furthermore, the Poisson’s ratio was taken as the ratio of transverse and applied strain increments, thereby giving the instantaneous metamaterial behavior,

$$\nu = -\frac{d}{d\varepsilon_a}(\varepsilon_t) \quad (3)$$

A uniaxial strain up to 60% was applied and the transverse strains, Poisson’s ratio, and reaction forces were extracted from the simulation results.

5. Design space of thin shell composite metamaterials

5.1. Controlling the deformation

A representative deformation under uniaxial tension of the FRP composite metamaterials is illustrated in Fig. 6(a), where the measured and simulated deformation is shown for a ‘reference’ sample up to 40% applied global strain. As originally conceived, the rotating square metamaterial contains an energy free mechanism in which the neighboring squares counter-rotate to create a bi-axial expansion [26]. The squares are assumed to be rigid and the hinges are infinitely small. Therefore, only an expansion of -1 Poisson’s ratio can be achieved without switching to rectangular hubs. In the adapted metamaterial studied here, the range of achievable behavior is expanded via the following two effects.

First, the finite extent of the ligaments allows the Poisson’s ratio to deviate from -1 significantly without breaking symmetry in the geometry of the metamaterial. As uniaxial tension is applied, the FRP ligaments act as hinges and begin to bend, causing rotation of the hubs. The ligaments parallel to the load direction see a combined axial and bending load. However, the ligaments transverse to the load direction, see only the opposing moments transferred to their ends by the two hubs to which they are attached and hence, are approximately loaded in pure bending (when neglecting edge effects in the metamaterial). This effect is demonstrated in Fig. 6(b), which plots the simulated ligament curvatures for various applied strains. The ligaments transverse to the load show constant curvature along their length even at high levels of applied strain and are under pure bending, whereas the ligaments parallel to the applied load show large variation of curvature along their length due to the combined bending and axial loading. Due to the higher curvature of the transverse ligaments, the deformation in the transverse direction is less than in the strained direction. This effect becomes more pronounced with increasing loading, causing the Poisson’s ratio to be a monotonically increasing function of the applied strain.

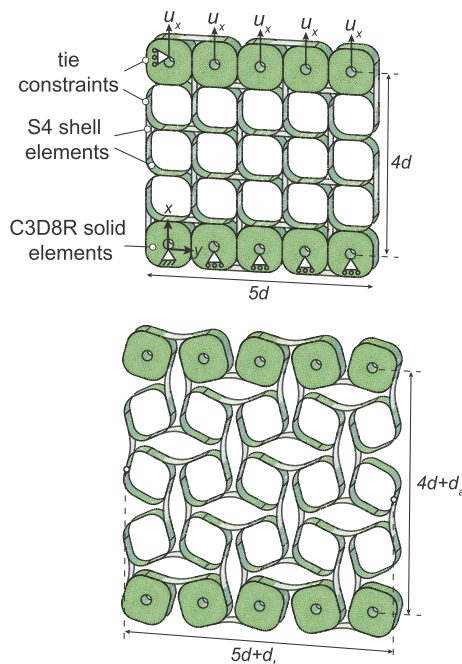


Fig. 5. Schematic of finite element model in unstrained and deformed configurations. The definition of the applied and transverse displacements, d_a and d_t , respectively, is illustrated.

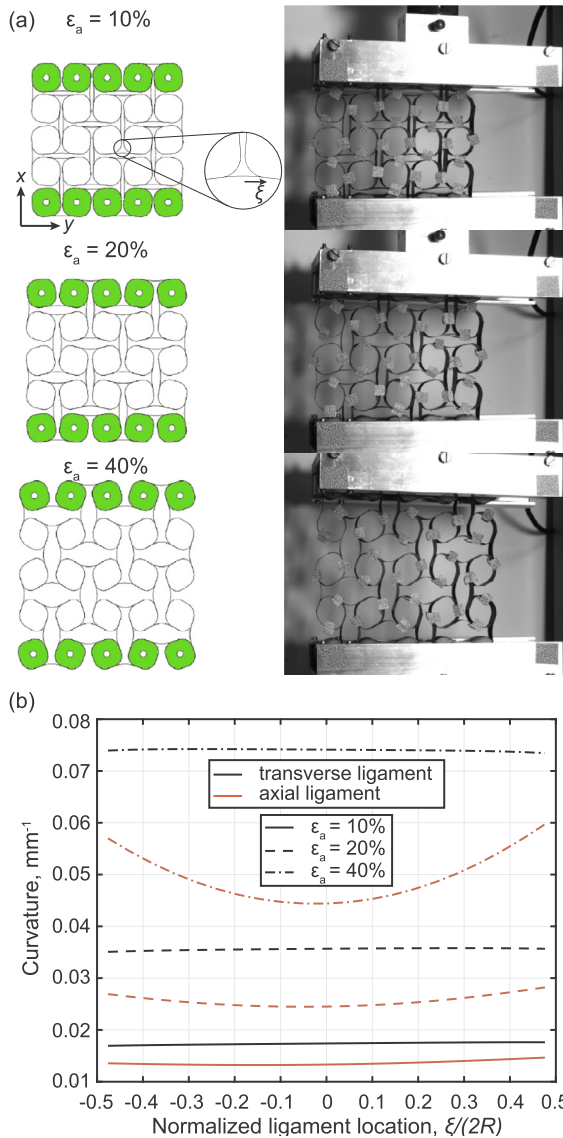


Fig. 6. (a) Representative deformation mode with cores removed for various applied strain levels. (b) Representative curvature of ligaments parallel to applied load and ligaments transverse to applied load for various applied strain levels. All data for ‘reference’ design.

Second, additional design freedom is offered by deformation of the hubs. In the presence of the polymer cores, the hubs rotate rigidly due to their significantly higher stiffness compared to the thin FRP ligaments. However, upon removal of the polymer cores, deformation of the FRP hubs is enabled at high strains. The ligaments parallel to the

loading direction apply an effective shear to the hubs (Fig. 6(a) at 40% strain). The amount of this shearing can be used to control the transverse expansion of the metamaterial and hence its Poisson’s ratio. The softer the hubs, the more they shear, bringing the Poisson’s ratio from $\nu = -1$ closer to zero.

The shear deformation of the hubs becomes particularly evident by tracking their dimensional changes as the metamaterial is strained. The hubs expand in one direction, d_1 , while flattening in the other, d_2 (Fig. 7(a)). This behavior is quite pronounced as the hubs can see dimensional changes of over 10% at an applied strain of 60%. Fig. 7(b) shows a comparison of the magnitude of this deformation for the ‘reference’ and ‘stiff hubs’ samples. The stiffer hubs show less pronounced shear in the 2-direction and the hub behavior is closer to rigid body motion.

Therefore, the finite extent of the ligaments as well as the finite hub stiffness allow for control of the elastic response and failure of the metamaterials as is illustrated next.

5.2. Elastic behavior

The measured metamaterial response until failure for all prototypes is compared to predicted performance in Figs. 8 and 9, showing the loading curves and instantaneous Poisson’s ratios, respectively. The experimentally measured Poisson’s ratio in Fig. 9 was smoothed using a moving-average filter to reduce noise stemming from numerically computing the derivative of experimental data as per Eq. 3.

All samples showed elastic behavior with no change in performance upon repeated loading cycles, thereby indicating the lack of macro-scale damage before structural failure began to occur. The repeated cycles are omitted for clarity. Furthermore, two nominally identical samples were tested for each design in Table 2 and exhibited repeatable elastic response.

Experiments show reasonable agreement with simulated performance for both the stiffness and Poisson’s ratios. Slight disagreements result due to the remaining friction between the bearings and rails, preventing the hubs from sliding uniformly. This results in slight drops in the load as the bearings slip and the prominent drops due to this effect are indicated by a star in Fig. 8 to differentiate this behavior from load drops due to failure.

All load curves in Fig. 8 show a non-linear stiffening behavior stemming from the parabolic relation between the applied displacement and the resulting hub rotation angle [26] and, hence, the curvature of the ligaments. Furthermore, increased tensile loading of the ligaments in the loading direction at high strains contributes to the non-linearity.

Intuitively, layups which are stiffer in bending show a stiffer response, with the maximum stiffness achieved by the ‘rigid hubs’ design and the lowest stiffness corresponding to the 45° anti-symmetric design with the lowest ligament bending stiffness.

The Poisson’s ratio of the metamaterial is controlled by the relative stiffness of the ligaments and the hubs (Fig. 9). Prototypes where the

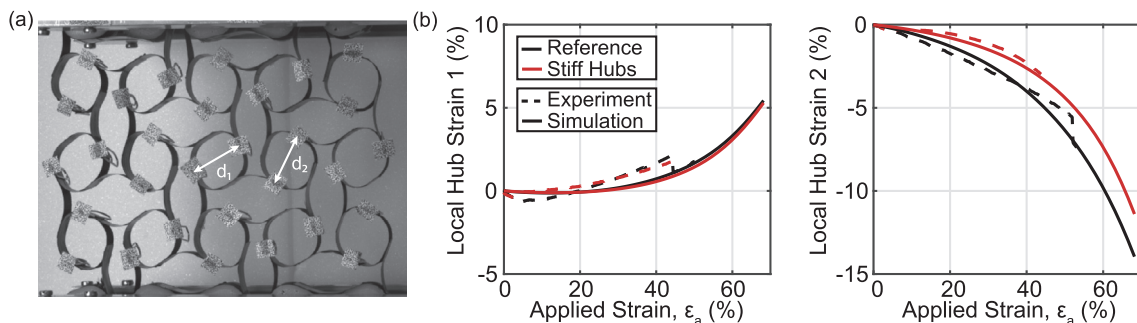


Fig. 7. (a) Definition of lengths used to compute the two local hub strains. (b) Hub strains for ‘reference’ and ‘stiff hubs’ samples.

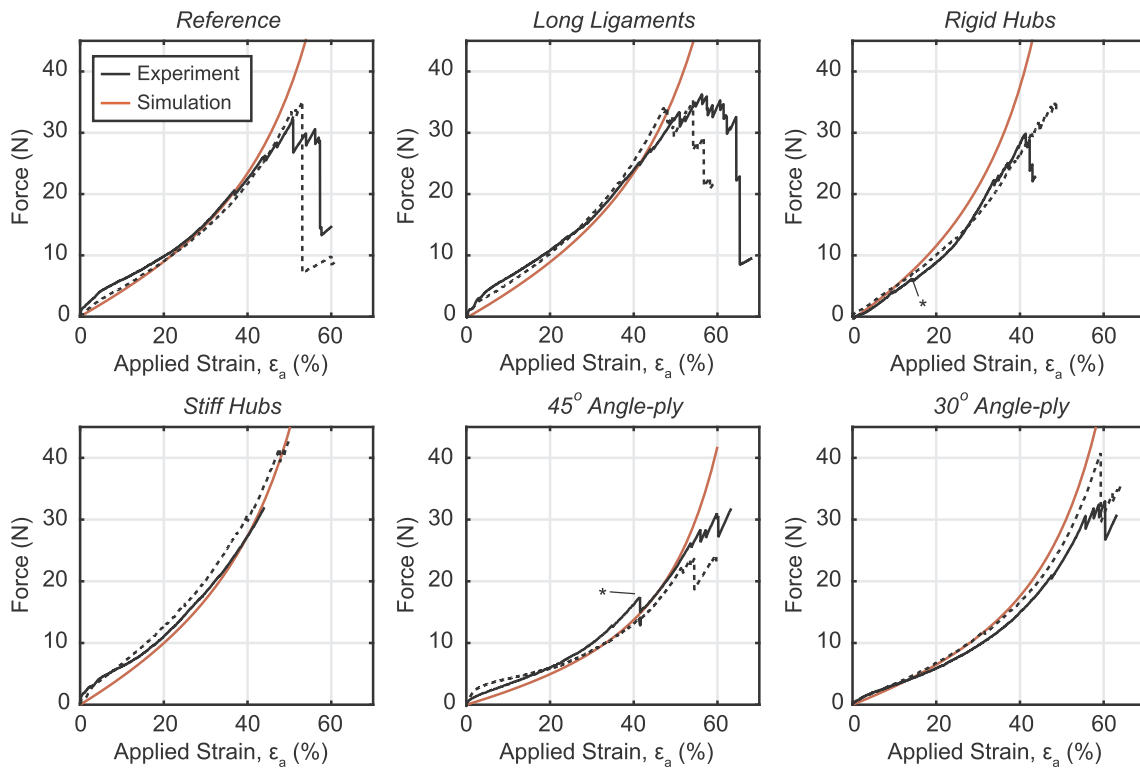


Fig. 8. Measured and simulated load curves as a function of applied strain, ϵ_a , for all tested samples.

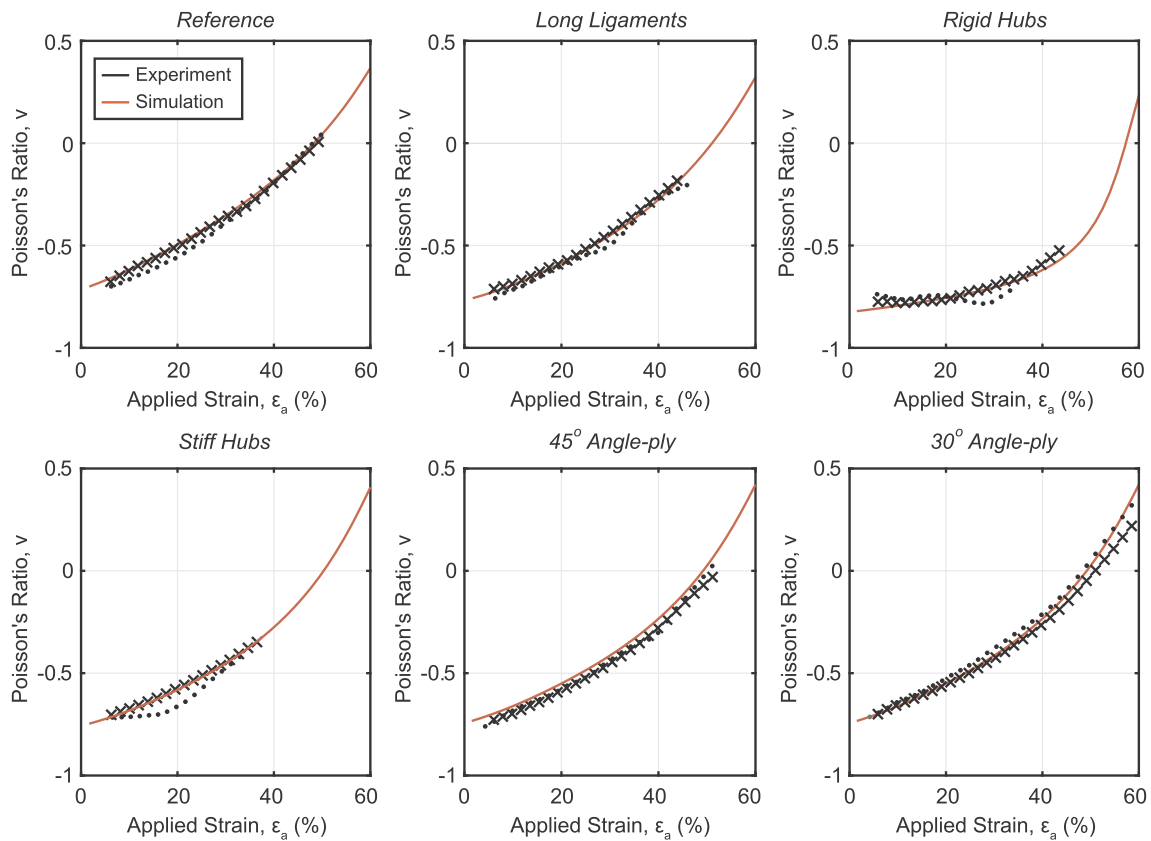


Fig. 9. Measured and simulated Poisson's ratio as a function of applied strain, ϵ_a , for all tested samples.

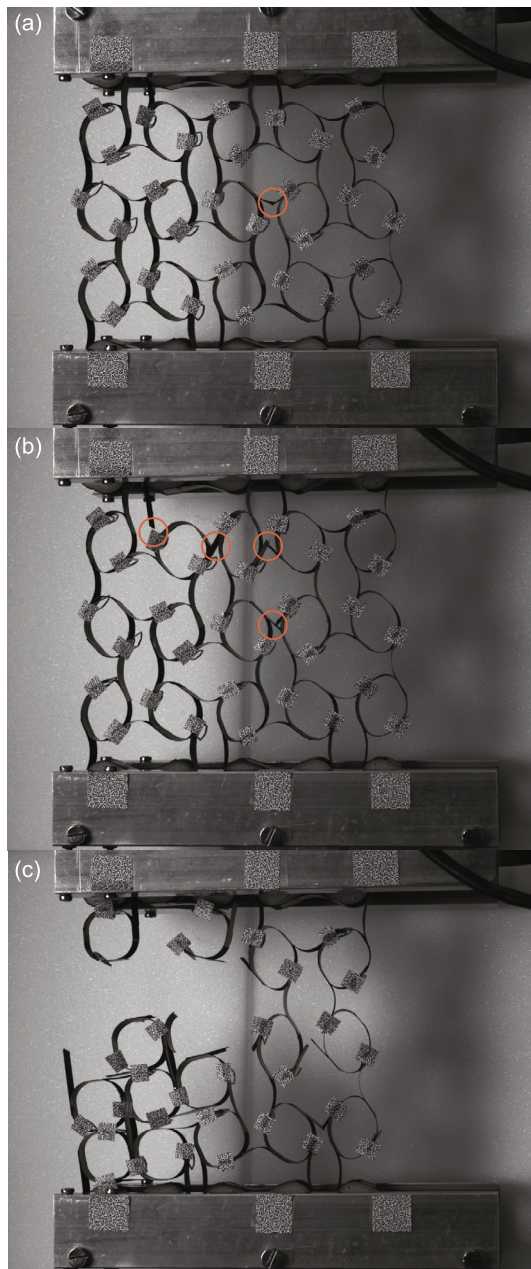


Fig. 10. Typical failure progression with ligament cracking highlighted in red. The ‘reference’ sample is pictured. (a) Initial failure of a single ligament. (b) Failure of multiple ligaments. (c) Ultimate failure due to ligament cracking and delamination of ligaments from hubs.

deformation is dominated by the bending of the ligaments, the Poisson’s ratio is closer to $\nu = -1$, that of the original rotating square mechanism. This is most evident in the ‘rigid hubs’ design, where the Poisson’s ratio remains relatively constant between $\nu = -0.8$ and $\nu = -0.65$ until strains over 40%. In this design, the variation from -1 Poisson’s ratio is due to the finite extent of the ligaments only as described in Section 5.1.

In the remaining samples, the deformation is a combination of ligament and hub deformation. The Poisson’s ratio exhibits much higher dependence on the applied strain than in the case of the rigid hubs. Both the finite ligaments and the hub deformations contribute to the resulting Poisson’s ratio as described in Section 5.1. In general, designs where the hubs are stiffer relative to the ligaments show a Poisson’s ratio closer to $\nu = -1$ since the hubs undergo less shear. This is evident comparing the ‘reference’ and ‘stiff hubs’ samples that show an average Poisson’s ratio of $\nu = -0.44$ and $\nu = -0.52$, respectively, over an applied strain range of 0–40%.

The introduction of thin composite shells into metamaterial geometries has enabled novel mechanics in the popular rotating square geometry. Control of the elastic parameters of the metamaterial has been achieved through the introduction of shear deformation in the hub shells by modification of the relative stiffness of the hub and ligament layouts. Moreover, it is interesting to note that at high strains the metamaterial is no longer auxetic (Fig. 9) and exhibits positive Poisson’s ratios. This effect can be leveraged to realize lightweight structures that switch between auxetic and non-auxetic behavior through their deformation.

5.3. Failure

Two different failure modes were observed in the metamaterials: cracking of the ligaments and delamination of the ligaments from the hubs. The former is governed by the flexural strength of the material, while the latter is triggered by a mode I fracture propagating between the ligaments and the hubs.

The failure in all samples began with the cracking of a single ligament transverse to the loading direction (Fig. 10(a)). These ligaments see the highest curvatures (Fig. 6)) and hence are the first to fail as the flexural strength for this material is significantly lower than its tensile strength [32]. The stresses in the structure are redistributed following the failure and so the cracking of a single ligament does not lead to catastrophic failure. As the applied strain continues to increase, further ligaments fail (Fig. 10(b)) until ultimate failure occurs via delamination of ligaments from the hubs (Fig. 10(c)).

A summary of the initial and ultimate failure strains for all samples is given by Table 3. Initial failure corresponds to a force drop in the load curve (except those a result of the bearings slipping), which can be accompanied in some cases by visible cracking of a single ligament. The values given are the average of the two samples tested for each design. The spread in failure strains between the two nominally identical samples stems from manufacturing imperfections, in particular, the variations in thickness seen in the composite (Fig. 3 panel B). Ply strains due to laminate bending scale with the distance from the neutral axis,

Table 3

Summary of strains and stresses at failure of tested samples. The initial and ultimate strains correspond to the metamaterial while the maximum ligament stresses at initial failure correspond to the stresses in the composite plies of the transverse ligaments.

Sample Name	Initial metamaterial failure strain (%)	Simulated ligament state at initial failure		Ultimate metamaterial failure strain (%)
		Max. stress in fiber direction (MPa)	Max. stress transverse to fibers (MPa)	
Reference	47.8	–1199 (0° ply)	13.0 (90° ply)	55.5
Long Ligaments	49.2	–1225 (0° ply)	12.9 (90° ply)	62.1
Stiff Hubs	42.0	–1157 (0° ply)	12.6 (90° ply)	47.0
Rigid Hubs	37.4	–1005 (0° ply)	10.6 (90° ply)	47.5
45° Angle-ply	52.4	–1015 (0° ply)	54.3 (–45° ply)	61.5
30° Angle-ply	57.5	–1118 (0° ply)	53.4 (–30° ply)	63.6

causing higher strains in thicker regions and, consequently, earlier failure.

The maximum stress failure criteria in combination with first-ply failure correlated with the initial ligament cracking in all samples. Typical strengths under a variety of loading conditions for M40J/epoxy composites, with a similar fiber volume fraction as in this work, can be found in literature. The expected tensile and compressive strengths in the fiber direction are approximately 2100–2450 MPa and 1200–1300 MPa, respectively [31,32]. Conversely, the reported tensile strength transverse to the fiber direction is quite low at only 30–53 MPa and can vary significantly depending on the fiber–matrix interface [34,32]. Therefore, it is expected that the longitudinal compressive and transverse tensile stresses in the ligaments transverse to the loading direction can induce failure. The simulated maximum compressive and transverse tensile stresses in the transverse ligaments at the experimentally obtained initial failure strains, as well as the plies in which they occur, are summarized in Table 3. The tensile strength in the fiber direction is not exceeded for any sample.

The failure of these complex structures is dependent on the ratio between the bending stiffness of the hub layup to that of the ligament layup. Designs which have the same stiffness ratio show initial failure at similar strain levels, as exemplified by the ‘reference’ and ‘long ligaments’ samples. The increased overlap between hubs and ligaments in the ‘long ligaments’ design delays only the ultimate failure. In these two designs, the transverse ligaments share a similar stress state at initial failure – they are roughly under pure bending with maximum compressive stresses of 1000–1200 MPa in the fiber direction in the outermost 0° ply (Table 3). This correlates with the compressive strength found in literature. As the hubs are stiffened relative to the ligaments, as in the ‘stiff hubs’ and ‘rigid hubs’ samples, the bending of the ligaments is more pronounced compared to the shearing of the hubs. Therefore, initial failure occurs at lower strains. The stress state of the transverse ligaments at initial failure remains similar to the other designs with a [0/90/0] layup.

This design principle is further demonstrated by the angle-ply laminates. For these designs, the initial failure strains at which the ligaments crack are increased by 5–10% compared to the ‘reference’ samples, despite a 33% increase in ligament thickness. For the 30° angle-ply layup, the hub stiffness is lower than that of the ligaments. As a result, the deformation becomes more localized to the hubs, which tend to shear (Section 5.1), thereby reducing bending in the ligaments and delaying initial failure to almost 60% applied strain. From Table 3, it can be seen that at initial failure both the maximum compressive strain in fiber direction (occurring in the 0° ply) and the transverse tensile stress (occurring in the –30° ply) are close to their strength values and all plies likely fail in rapid succession causing ligament cracking.

Overall, the compressive and transverse strengths of the material show a good correlation with experimentally observed first-ply failures of the metamaterial ligaments. However, further examination is required to identify precisely the failure mechanism in the thin-ply composites and is beyond the scope of this work. Moreover, the repeatable failure progression and agreement with expected elastic and failure behavior points to the high quality of the fabricated prototypes. The demonstrated elastic strain limits of the novel metamaterials developed here significantly exceed those of existing FRP metamaterials and can even rival those of polymeric designs [1]. Moreover, the anisotropy of the thin FRP shells can offer stiff structural response in compression and bending, unlike designs comprised of soft polymers. Therefore, this work sets the stage for further investigation of the application of composite metamaterials to shape adaptation in lightweight, load-carrying structures.

6. Conclusion and outlook

This study addressed the challenge of fabricating complex composite metamaterial assemblies for application to morphing in

lightweight, load-carrying structures. A novel integrated fabrication process for cellular mechanical metamaterials consisting of FRP shells was presented that utilized additively manufactured tooling. Furthermore, the technique eliminates the need for adhesive bonding of individually cured shell components by using silicone spacers to apply pressure everywhere in the metamaterial assembly and thereby co-cure all components in a single manufacturing step. The procedure has the potential to reduce fabrication times and metamaterial mass, and enable extreme strains in composite metamaterials. The proposed fabrication technique yields structures of high quality with predictable and repeatable mechanical behavior.

The integral fabrication technique is not limited to the geometry studied in this paper and is sufficiently broad to be applied to any shell-based metamaterial geometry including the commonly used chiral geometries found in literature. Most importantly, the use of 3D printed composite tooling allows for rapid, cost-efficient prototyping and enables the fabrication of aperiodic metamaterials without the cost associated with fabrication of a large number of custom molds.

More significantly, successful integral fabrication of composite metamaterials has enabled their practical use for expanding the set of achievable mechanical performance. The concept under study has revealed novel mechanics by allowing the superposition of the controlled deformation of the individual shell components – namely, the hubs and ligaments. Through selection of the relative hub bending stiffness compared to that of the ligaments, easily achievable in practice for laminated FRP shells, tuning of global deformation and failure of the metamaterial were demonstrated. This is an attractive feature when precise control of the deformation is required for example to interface the metamaterial to another structure.

Moreover, the anisotropy of the FRP material was leveraged to achieve new properties. Tuning of the composite layup has allowed for realization of composite metamaterials which undergo 60% deformation elastically – an unprecedented property for composite metamaterials. This can enable the use of such materials for shape morphing in load carrying structures to achieve high deformability in the tensile direction, and high stiffness in compression or bending.

The novel mechanics introduced by allowing hub deformation is a further area of interest. The hub and ligament features are common to many mechanical metamaterial geometries, including those with rotating polygons, many chiral configurations, and the re-entrant star patterns. In these ideal configurations, the hubs are considered rigid but by allowing their deformation, an unprecedented design space is opened. Not only can the metamaterial elastic coefficients be tailored but the load-curves can be designed to be linear or non-linear across a large strain range, and out-of-plane deformation can be induced by exploiting the anisotropy of the composite shells. Through this feasibility study, a novel area of investigation has been opened on the use of composite anisotropy in mechanical metamaterials.

Data Availability

The data supporting the experimental and numerical results in this study is available from the corresponding author upon reasonable request.

Declaration of Competing Interest

The authors declare that they have no known competing financial interests or personal relationships that could have appeared to influence the work reported in this paper.

Acknowledgment

This work was supported by the ETH Zürich Postdoctoral Fellowship Program, cofounded by the Marie Curie Actions for People COFUND

Program. The SNF R'Equip program, SNF 206021_150729, has supported the acquisition of the Digital Image Correlation equipment used in this study.

References

- [1] Bertoldi K, Vitelli V, Christensen J, Van Hecke M. Flexible mechanical metamaterials. *Nat Rev Mater* 2017;2:17066. <https://doi.org/10.1038/natrevmats.2017.66>.
- [2] Neville RM, Scarpa F, Pirrera A. Shape morphing Kirigami mechanical metamaterials. *Sci Rep* 2016;6:31067. <https://doi.org/10.1038/srep31067>.
- [3] Lv C, Krishnaraju D, Konjevod G, Yu H, Jiang H. Origami based mechanical metamaterials. *Sci Rep* 2014;4:5979. <https://doi.org/10.1038/srep05979>.
- [4] Coulais C, Teomy E, De Reus K, Shokef Y, Van Hecke M. Combinatorial design of textured mechanical metamaterials. *Nature* 2016;535(7613):529–32. <https://doi.org/10.1038/nature18960>.
- [5] Haghpanah B, Salari-Sharif L, Pourrajab P, Hopkins J, Valdevit L. Multistable shape-reconfigurable architected materials. *Adv Mater* 2016;28(36):8065. <https://doi.org/10.1002/adma.201670255>.
- [6] Schaedler TA, Carter WB. Architected cellular materials. *Annu Rev Mater Res* 2016;46(1):187–210. <https://doi.org/10.1146/annurev-matsci-070115-031624>.
- [7] Surjadi JU, Gao L, Du H, Li X, Xiong X, Fang NX, Lu Y. Mechanical metamaterials and their engineering applications. *Adv Eng Mater* 2019;21(3):1–37. <https://doi.org/10.1002/adem.201800864>.
- [8] Yang D, Mosadegh B, Ainla A, Lee B, Khashai F, Suo Z, Bertoldi K, Whitesides GM. Buckling of elastomeric beams enables actuation of soft machines. *Adv Mater* 2015;27(41):6323–7. <https://doi.org/10.1002/adma.201503188>.
- [9] Shintake J, Cacucciolo V, Floreano D, Shea H. Soft robotic grippers. *Adv Mater* 2018;30(29):1–33. <https://doi.org/10.1002/adma.201707035>.
- [10] Ali MN, Busfield JJC, Rehman IU. Auxetic oesophageal stents: dtructure and mechanical properties. *J Mater Sci Mater Med* 2014;25(2):527–53. <https://doi.org/10.1007/s10856-013-5067-2>.
- [11] Kim D-J, Jo E-S, Cho Y-K, Hur J, Kim C-K, Kim CH, Park B, Kim D, Choi Y-K. A frequency reconfigurable dipole antenna with solid-state plasma in silicon. *Sci Rep* 2018;8:14996. <https://doi.org/10.1038/s41598-018-33278-1>.
- [12] Zhang H, Guo X, Wu J, Fang D, Zhang Y. Soft mechanical metamaterials with unusual swelling behavior and tunable stress-strain curves. *Sci Adv* 2018;4(6):1–11. <https://doi.org/10.1126/sciadv.aar8535>.
- [13] Airoidi A, Bettini P, Panichelli P, Oktem MF, Sala G. Chiral topologies for composite morphing structures – Part I: Development of a chiral rib for deformable airfoils. *Phys Status Solidi Basic Res* 2015;252(7):1435–45. <https://doi.org/10.1002/pssb.201451689>.
- [14] Bettini P, Airoidi A, Sala G, Landro LD, Ruzzene M, Spadoni A. Composite chiral structures for morphing airfoils: numerical analyses and development of a manufacturing process. *Compos Part B Eng* 2010;41(2):133–47. <https://doi.org/10.1016/j.compositesb.2009.10.005>.
- [15] Cramer NB, Cellucci DW, Formoso OB, Gregg CE, Jenett BE, Kim JH, Lendraitis M, Swei SS, Trinh GT, Trinh KV, Cheung KC. Elastic shape morphing of ultralight structures by programmable assembly. *Smart Mater Struct* 2019;28(5):055006. <https://doi.org/10.1088/1361-665x/ab0ea2>.
- [16] Nisser MN, Izzo D, Orggraeae AB. An electromagnetically actuated, self-reconfigurable space structure. *JSASS Aerosp Tech Japan* 2017;14:1–9.
- [17] Ochalek M, Formoso O, Trinh G, Jenett B, Cheung K. Geometry and Joint Systems for Lattice-Based Reconfigurable Space Structures. In: 2019 IEEE Aerosp. Conf., Big Sky, MT, USA; 2019. <https://doi.org/10.1109/AERO.2019.8742178>.
- [18] Underwood C, Pellegrino S, Priyadarshan H, Simha H, Bridges C, Goel A, Talon T, Pedivellano A, Leclerc C, Wei Y, Royer F, Ferraro S, Sakovsky M, Marshall M, Jackson K, Sommer C, Vaidhyanathan A, Sooraj V, Baker J. AAReST Autonomous Assembly Reconfigurable Space Telescope Flight Demonstrator. In: 69th Int. Astronaut. Congr., Bremen, Germany; 2018. p. IAC-18-A6.5.2.
- [19] Murphey TW, Peterson ME, Grigoriev MM. Large strain four-point bending of thin unidirectional composites. *J Spacecr Rockets* 2015;52(3):882–95. <https://doi.org/10.2514/1.A32841>.
- [20] Daniel IM, Ishai O. *Engineering mechanics of composite materials*. 2nd ed. Oxford University Press; 1994.
- [21] Barber RB, Hill CS, Babuska PF, Wiebe R, Aliseda A, Motley MR. Flume-scale testing of an adaptive pitch marine hydrokinetic turbine. *Compos Struct* 2017;168:465–73. <https://doi.org/10.1016/j.compstruct.2017.02.051>.
- [22] Daynes S, Weaver PM, Potter KD. Aeroelastic study of bistable composite airfoils. *J Aircr* 2009;46(6):2169–73. <https://doi.org/10.2514/1.44287>.
- [23] Arrieta AF, Kuder IK, Waeber T, Ermanni P. Variable stiffness characteristics of embeddable multi-stable composites. *Compos Sci Technol* 2014;97:12–8. <https://doi.org/10.1016/j.compscitech.2014.03.017>.
- [24] Pellegrino S, Folding and Deployment of Thin Shell Structures. In: Bigoni D (editor), *Extrem. Deform. Struct.*, Springer; 2015. p. 179–267. https://doi.org/10.1007/978-3-7091-1877-1_5.
- [25] National Research Council of the National Academies, *Decadal Survey of Civil Aeronautics*, The National Academies Press, Washington D.C.; 2006.
- [26] Grima JN, Evans KE. Auxetic behavior from rotating squares. *J Mater Sci Lett* 2000;19(17):1563–5. <https://doi.org/10.1023/A:1006781224002>.
- [27] Rotima AG, FEP Schrumpfschlauch 1,3:1 Data Sheet, Tech. rep.; 2019.
- [28] Schlothauer A, Royer F, Pellegrino S, Ermanni P. Flexible Silicone Molds for the Rapid Manufacturing of Ultra-Thin Fiber Reinforced Structures. In: *SAMPE Conf. Proc.*, Long Beach, CA; 2018.
- [29] Apium Additive Technologies, *Additive Manufacturing Solutions from Apium*; 2018. URL: <https://apiumtec.com/en/additive-manufacturing>.
- [30] Victrex, PEEK 450G data sheet, Tech. rep.; 2014.
- [31] North Thin Ply Technologies, NTPT Thinpreg 513 Data Sheet, Tech. rep.; 2017.
- [32] Toray Carbon Fibers America, M40J Data Sheet, Tech. rep.; 2017.
- [33] Dassault Systemes, Abaqus 6.14 Documentation, Tech. rep.; 2018.
- [34] Maurin R, Davies P, Baral N, Baley C. Transverse properties of carbon fibres by nano-indentation and micro-mechanics. *Appl Compos Mater* 2008;15(2):61–73. <https://doi.org/10.1017/CHO9781139524377.001>.